Ulinastatin improves renal microcirculation by protecting expression of VE-cadherin and inhibiting autophagy in a septic rat model

Tian Li
Capital Medical University Affiliated Beijing Friendship Hospital
Xiao-jun Ji
Capital Medical University Affiliated Beijing Friendship Hospital
Jing-feng Liu
Capital Medical University Affiliated Beijing Friendship Hospital
Xin-jie Guo
Capital Medical University Affiliated Beijing Friendship Hospital
Ran Pan
Capital Medical University Affiliated Beijing Friendship Hospital
Hai-zhou Zhuang
Capital Medical University Affiliated Beijing Friendship Hospital
Lei Dong
Capital Medical University Affiliated Beijing Friendship Hospital
Mei-li Duan
Capital Medical University Affiliated Beijing Friendship Hospital
Ang Li (liang@ccmu.edu.com)
Capital Medical University https://orcid.org/0000-0002-1478-3072

Research

Keywords: sepsis-associated acute kidney injury, microcirculation, ulinastatin, vascular endothelial-cadherin, autophagy

Posted Date: April 6th, 2021

DOI: https://doi.org/10.21203/rs.3.rs-372806/v1

Abstract

Background: Increased permeability of the renal capillary is a common consequence of sepsis-associated acute kidney injury. Vascular endothelial (VE)-cadherin is a strictly endothelial-specific adhesion molecule that can control the permeability of the blood vessel wall, and autophagy plays an important role in maintaining cell stability. Ulinastatin, a urinary trypsin inhibitor, attenuates the systemic inflammatory response and visceral vasopermeability. However, it is uncertain whether ulinastatin can improve renal microcirculation by acting on the adhesion junction.

Methods: We obserned the effect of Ulinastatin in the septic rat model by using contrast-enhanced ultrasonography (CEUS) to evaluate perfusion of the renal cortex and medulla. Male adult Sprague-Dawley rats were subjected to cecal ligation and puncture and divided into the sham, sepsis, and ulinastatin groups. Ulinastatin (50 000 U/kg) was injected into the tail vein 1 hour after the operation. At 24 hours postoperatively, CEUS was performed to evaluate the renal microcirculation blood flow and microcirculation perfusion. Histological staining was used to evaluate kidney injury scores. Western blotting was used to assess the expression of VE-cadherin and LC3II, peripheral serum cytokines (interleukin [IL]-1β, IL-6, and tumor necrosis factor-α levels), renal function (creatinine, urea nitrogen, and S-thrombomodulin level), and the urine neutrophil gelatinase-associated lipocalin level.

Results: Compared with sham group, ulinastatin reduced the inflammatory response, maintained the expression of VE-cadherin, inhibited autophagy, and meliorated cortical and medullary perfusion.

Conclusions: Ulinastatin effectively protects the adhesion junction and helps to ameliorate the perfusion of kidney capillaries during sepsis by inhibiting autophagy and the expression of inflammatory factors.

Introduction

Sepsis-associated acute kidney injury (S-AKI) is a very common complication in critically ill patients; it is associated with prolonged length of hospital stay and a huge cost, and increases the mortality and risk of developing chronic kidney disease[1-4]. The etiology of S-AKI is complex and poorly understood. Previous studies have suggested that ischemia–reperfusion (IR) is the main cause of acute kidney injury (AKI) in sepsis, and with the development of fluid resuscitation therapy; it has been found that in the early stage of sepsis, the total blood flow of the kidney remains unchanged or increased, but AKI may still occur[5]. Now, it is clear that S-AKI is obviously different from ischemic AKI both in the experimental setting and in the clinical setting[6]. Several pathophysiological mechanisms have been proposed for S-AKI, such as vasodilatation-induced glomerular hypoperfusion, peritubular capillary network dysregulation, inflammatory reactions, and oxidative stress[7, 8]. Increasing evidence suggests an integrative physiological compartment where these mechanisms come together: renal microcirculation[9].

Endothelial dysfunction plays a central role in microcirculatory dysfunction during S-AKI[10]. Endothelial cell-to-cell junctions play crucial roles in maintaining intercellular adhesion, transferring intracellular signals, and modulating contact inhibition of cell growth[11].Therefore, disruption of endothelial

junctions may increase vascular permeability by opening intercellular gaps[12]. Vascular endothelial (VE)-cadherin is a strictly endothelial-specific adhesion molecule that controls the permeability of the blood vessel wall for cells and substances[13]. Autophagy is an evolutionary conserved mechanism that enables the delivery and direct targeting of cytoplasmic materials to the lysosome for degradation and recycling[14]. Research in the past few years has shown the induction of autophagy in proximal tubular cells[15] and maintenance of the integrity of glomerular capillaries during AKI[16]. The relationship between the expression of VE-cadherin and autophagy is not yet clear.

Ulinastatin, a urinary trypsin inhibitor and a potent multivalent Kunitz-type serine protease inhibitor derived from human urine, has been shown to control a series of pro-inflammatory mediators and cytokines[17]. Recently, studies have shown that ulinastatin has been widely used as a renal protective drug in patients with septic shock and ischemia[18, 19]. In S-AKI, the effect of ulinastatin on renal microcirculation perfusion remains unclear.

Microcirculation is a functionally independent network of vessels that encompasses arterioles, venules, and capillaries, with diameters ranging from 5 μm to 100 μm[20]. The pathophysiology of microcirculation can clarify the intricacies involved in tissue perfusion. Renal dysfunction is also known to be associated with a significant change in perfusion[21], but there is no clear conclusion about the perfusion of renal tissue in S-AKI.

Contrast-enhanced ultrasonography (CEUS) is a promising technology that has been validated to assess and quantify microcirculation up to capillary perfusion[22]. The contrast agents are microbubbles made of gases embedded within a shell that can function as red blood cell tracers. This technology allows for continuous imaging of the vasculature and blood flow[23]. In the present study, we used CEUS to evaluate perfusion of the renal cortex and medulla in a septic rat model.

Materials And Methods

Experimental animals

Experiments were performed using male Sprague-Dawley rats (body weight, 250–300 g) with the approval of the Bioethics Committee of Beijing Friendship Hospital, Capital Medical University. Rats were housed three per cage in a room with an environment temperature of 21–24°C with a 12:12-hour light–dark cycle and were fed standard rat chow with ad libitum access to water. Rats were fasted for 12 hours before surgery.

Establishment of the septic rat model and treatment

Sepsis was induced by cecal ligation and puncture (CLP), as described previously[20] to establish a rat model of abdominal infection after surgery. An intraperitoneal injection with 10% chloral hydrate at 0.03 mL/100 g for anesthesia was used to maintain spontaneous breathing, and the animal was placed supine on the heated platform that can maintain the temperature at 37°C. A longitudinal skin midline

incision was made with a scalpel, being careful not to penetrate the peritoneal cavity, and then small scissors were used to extend the incision and to gain entry into the peritoneal cavity (3–4 cm). The linea alba was identified, and we made an intermuscular incision. When locating the cecum and exteriorizing it, it is critical not to breach or damage the mesenterial blood vessels. The membrane was dissected at the mesenteric site of the cecum, and the cecum was ligated at half the distance between the distal pole and the base of the cecum (mid-grade sepsis). The cecal contents were gently pushed toward the distal cecum, and at the time of cecal puncture using 18-gauge needles, we gently aspirated any trapped air or gases to avoid puncturing blood vessels. After removing the needle, we extruded a droplet of feces from both the mesenteric and antimesenteric penetration holes to ensure patency. We moved the cecum into the abdominal cavity, and closed the peritoneum, fasciae, and abdominal musculature with wax-coated braided silk nonabsorbable surgical sutures 4-0. Animals were resuscitated by injecting prewarmed normal saline (37°C, 5 mL per 100 g body weight) subcutaneously to demonstrate the early, hyperdynamic phase of sepsis. Rats were returned to their cages immediately at the end of the surgical procedures where access to water and food was available.

Rats were divided into three groups: sham group, the cecum was squeezed gently (no perforation) and was injected with the same volume of 0.9% saline via the tail vein; sepsis group, the steps are described above; and ulinastatin group, rats were treated with 50 000 U/kg/24 h of ulinastatin via the tail vein immediately after the operation.

Hemodynamic measurements

We measured the blood pressure and heart rate of rats with a rat tail blood pressure monitor (BP-98A, Softron, Tokyo, Japan). Blood lactic acid was measured using a portable blood lactate meter (YK-Scout, Germany).

Assessment of renal microcirculation perfusion

All rats were anesthetized with 3% isoflurane in oxygen before imaging. The rats were placed on the ventral side of the heated imaging platform after anesthesia was induced. Anesthesia was maintained by delivering 1%–2% isoflurane in oxygen through a nose cone during imaging. We used the Vevo 2100 ultrasound system (FujiFilm VisualSonics Inc., Toronto, Canada) in B-mode. We placed the MS-400 probe in the renal artery to measure the width of the renal artery, and used the M-mode to measure the arterial flow rate. The analysis indices were the renal artery resistance index (RI) and average blood flow velocity. We set the relevant parameters as follows: frequency, 30 MHz; power, 100%; frame rate, 12; gain, 28.0 dB; dynamic range, 60 dB; and depth, 7.07 mm.

The unit was equipped with an MS250 transducer, and we used a wide beam width setting to ensure a low, uniform transmission pressure for all depths. We set the relevant parameters as follows: frequency, 18 MHz; energy, 10%; frame rate, 36; contrast gain, 37.0 dB; two-dimensional gain: 18.0 dB; depth, 20 mm; and dynamic range, 35 dB.

The focus range was placed in the middle of the left kidney, and 5 mL of physiological saline was injected into the ultrasonographic contrast agent (SonoVue lyophilized powder; Bracco, Milan, Italy) according to the manufacturer's instructions, and shaken to form a sulfur hexafluoride microbubble suspension. We withdrew 0.2 mL/150 g of rat body weight, and injected a rapid bolus into the tail vein of each rat using a dedicated syringe pump, followed by physiological saline (0.5 mL). Following the contrast injection, we recorded 500 frames and analyzed the stored dynamic images offline using Vevo LAB (VisualSonics, Inc.) and Vevo CQ software (nonlinear amplitude modulation contrast imaging, VisualSonics, Inc.).

The cortical and medullary regions of interest were evaluated at the same depths and positions, as much as possible, over a 0.4-mm^2 area, and the time intensity curve was plotted. The analysis indicators were the peak enhancement (PE), representative of blood volume, mean transit time (mTT), renal resistance index (RI), pulse index (PI), and wash-in perfusion index (WiAUC/RT), representative of blood flow. All parameters were measured three times and averaged.

Enzyme-linked immunosorbent assay

Blood and urine samples were obtained. Renal function was monitored by measuring the concentration of creatinine (E02C0629, Bluegene) and blood urea nitrogen (E02C0697, Bluegene) in serum using enzyme-linked immunosorbent assay (ELISA) kits. We measured the neutrophil gelatinase-associated lipocalin (NGAL) level using rat NGAL ELISA kits (ab119602, Abcam, Cambridge, UK). Serum levels of tumor necrosis factor (TNF)-α (ab46070, Abcam), interleukin (IL)-1β (ab100767, Abcam), and IL-6 (ab119548, Abcam) were detected using a rat bioactive ELISA assay.

Contrast-enhanced ultrasonography of the kidney

We performed CEUS at four time points (3, 6, 12, and 24 hours). By injecting the contrast agent via the tail vein of the rats in the sham group, the contrast agent rapidly reached the renal cortex, and the medullary echo from the renal sinus along the renal arteries was visible. Eventually, the entire renal cortex and medulla formed a "fireball-like" enhancement and then began to subside, and the cortex subsided last.

Histological examination and kidney Paller score

The left kidney was isolated and fixed by immersion in 4% paraformaldehyde, embedded in paraffin, and sectioned at a thickness of 4 μm. Following hematoxylin and eosin staining, pathological changes in kidney cortical and medullary tissues were examined under a light microscope, and slides were reviewed blindly and scored on a semiquantitative scale to evaluate changes found in acute renal failure.

We used the Paller score to assess the severity of renal tubular injury. Slides were reviewed blindly and scored on a semiquantitative scale. Ten high-power fields were randomly selected under a light microscope, avoiding repeated scoring of different convolutions of the same tubule, and renal tubular injury was evaluated according to the Paller score. Higher scores represented more severe damage

(maximum score per tubule was 10), with points given for the presence and extent of tubular epithelial cell flattening, dilated renal tubules (1 point), brush border injury, shedding (1 or 2 points), cytoplasmic vacuolization (1 point), interstitial edema (1 point), cell membrane bleb formation, cell necrosis, and tubular lumen obstruction (1 or 2 points)[24].

Western blotting

The left kidney obtained from each group was frozen in liquid nitrogen and stored at -80°C. Tissue samples from various groups were homogenized using a protein extraction reagent containing protease inhibitors. In brief, protein samples were electrophoresed on 4%–12% SDS-PAGE polyacrylamide gels, incubated with the appropriate antibodies (VE-cadherin Rabbit mAb, ab231227, Abcam), LC3II (E5Q2K) Mouse mAb (#83506, CST), and measured using an enhanced chemiluminescence detection system. Densitometric analysis was performed using ImageJ software (National Institutes of Health, Bethesda, MD).

Statistical analysis

Statistical analyses were performed using SPSS 22.0. The data are expressed as the mean ± SD. After homogeneity test of variances, one-way analysis of variance (ANOVA) followed by multiple comparison of the Tukey test was used to determine the statistical significance of different groups. All experiments were conducted at least in triplicate from different cell or tissue samples. Differences were considered statistically significant at $P < 0.05$.

Results

Systemic hemodynamics and renal function

The mean arterial pressure (MAP) fluctuated between 100 and 110 mmHg in the sham group, with a slight and transient increase, which presented a state of high dynamics in the early stage of sepsis (Fig.1A). This change in the MAP was very significant at 6 hours after surgery, and then the MAP gradually decreased, reaching the lowest level at 24 hours. At 12 hours and 24 hours after surgery, the MAP was statistically different between the sepsis and sham groups ($P < 0.05$). At 48 hours postoperatively, the MAP gradually increased, but it still did not return to the baseline level (Fig.1A). After the intervention with ulinastatin, the increase in the MAP at 6 hours after surgery was lower than that in the sepsis group; at 24 hours after the operation, the MAP of the ulinastatin group was higher than that of the sepsis group, and there was a statistically significant difference ($P < 0.05$). In the sham group, the heart rate increased within 6 hours, and the preliminary consideration was that the heart rate changes were related to the day and night of rats (Fig.1B). Compared with the sham group, the heart rate of the sepsis group increased within 3 hours, and then it gradually decreased by the next time point, reaching the lowest level at 24 hours. Changes in the heart rate were similar to those of MAP. In the ulinastatin group, the heart rate was similar to that of the sham group (Fig.1B).

The normal lactate level was 0.8–1.3 mmol/L. There was no statistically significant difference in lactate levels between the three groups of rats at 0-6 hours after surgery. Lactate levels increased at 12 hours and then reached a peak at 24 hours (3.6 mmol/L) in the sepsis group (Fig. 1C). Compared with the sepsis group, the lactate level in the ulinastatin group was lower at 12 and 24 hours (Fig. 1C). Figure 1 shows that ulinastatin improved the macroscopic hemodynamics of septic rats. Figure 2 shows the abnormal renal function in the septic rats. In the sepsis group, the creatinine level gradually increased at 3-6 hours, and the increase in creatinine at this time was considered to be related to mixed factors such as surgery, rehydration, and anesthesia. The creatinine level decreased within 12 hours, then gradually increased, and reached its peak at 24 hours. There was a statistically significant difference in the creatinine level between the sepsis and sham groups (Fig. 1D). In the sepsis group, the urea nitrogen level gradually increased and was twice that of the sham group at 24 hours (Fig. 1E). Blood urea nitrogen levels were lower in the ulinastatin group than in the sepsis group. In the sepsis group, S-thrombomodulin (S-TM) levels were higher than those in the sham group, especially at 3 hours and 24 hours (Fig. 1F). The urine NGAL level increased most obviously after 3 hours, and then gradually decreased (Fig. 1G).

Ulinastatin reduces the expression of inflammatory factors

In the sepsis group, we observed a significant increase in the levels of inflammatory factors. IL-6 levels increased significantly at 3 hours and 12 hours, and there was a statistical difference between the sepsis and ulinastatin groups (Fig. 2). The IL-1β level increased obviously at 3 hours and 24 hours, but there was no statistical difference between the sepsis and ulinastatin groups. The level of TNF-α, a multidirectional pro-inflammatory cytokine, increased significantly in the early postoperative period, then gradually decreased, and significantly reduced inflammatory factors at 3 hours and 6 hours.

Contrast-enhanced ultrasonography of the kidney

The time to peak (TTP) enhancement was approximately 2–3 seconds, and it dissipated after 30 seconds (Fig. 3A). Perfusion estimates in Vevo CQ are made by a curve-fitting process that adjusts the parameters of a mathematical model function to best fit the experimental linearized signal. In the context of ultrasound contrast imaging, the mathematical function is called the perfusion model (Fig. 3B). The model serves to estimate a set of perfusion parameters for quantification purposes that can be divided into three categories: amplitude (PE, etc.), time (rise time [RT], mTT, etc.), and a combination of amplitude and time (WiR). The intensity before the contrast agent reached the renal parenchyma was set to zero, and the cumulative intensity was calculated. The contrast agent intensity is encoded by a particular color on the parameter color scale. The rat medulla is shown in cyan and blue, and the cortex is shown in red and yellow (Fig. 3C), illustrating the position of the regions of interest in the renal cortex (continuous yellow line) and renal medulla (red dashed line), avoiding inclusion of the arteries. In the sham group, the outlines of the cortex and medulla were clear, and the cortical and medullary PE values were 32 dB and 10 dB, respectively. The mean velocity of the renal artery was 350 mm/s. In the sepsis group at 24 hours, part of the renal parenchyma was not filled with contrast agent, the mean velocity in the renal artery decreased to 160 mm/s, and the outlines of the cortex and medulla were no longer clear (Fig. 3C). The

renal artery blood flow (RBF) was calculated by measuring the diameter of the renal artery (d) and the average blood flow velocity (TAV) of the renal artery using the formula: $A = (\pi d^2 / 4) \times TAV$. In the sepsis group, RBF increased at 6 hours and 12 hours (Fig. 3D), but the MAP began to decrease after 12 hours. Therefore, the change in renal artery blood flow was later than the change in the MAP. We also measured the RI of the renal artery and the vascular PI. In the sepsis group, the RI gradually decreased and was accompanied by a decrease in the PI. These findings imitated the hemodynamic characteristics of septic patients who have a high cardiac output and low resistance, and the PI of the renal artery worsened (Fig. 3D).

Under these conditions, we further measured the blood perfusion of the cortical medulla of the kidney. The trend of the cortical PE change was consistent with the trend of the RBF. Compared with the sham group, PE in the sepsis group showed no obvious change before 12 hours, and there was a significant decrease at 24 hours (Fig. 3E). The change of renal medulla blood flow was earlier than that of the cortex, and it began to decrease significantly at 12 hours in the sepsis group. It seemed that medullary perfusion was more related to the MAP, whereas cortical perfusion was related to the RBF (Fig. 3E). The change in the WiAUC/RT was parallel to that in the PE. The mTT measured the average time that blood takes to transit through a portion of the tissue. Cortical mTT was prolonged first at 6 hours; at the same time, the TTP was shortened, so the time of outflow was prolonged (Fig. 3F). The cortical mTT returned to the baseline level at 12 hours, so we considered that mTT extension at 6 hours was related to the previous fluid supplementation. The cortical mTT was prolonged secondly at 24 hours, and the TTP was prolonged, which may be related to microvascular changes. The medullary mTT persisted for 12 hours (Fig. 3F), and there was no recovery period again, so we speculated that there were already microvascular abnormalities. After ulinastatin treatment, we observed no obvious increase in the RBF, RI, and PI at 24 hours. This may be related to the inhibition of the expression of inflammatory factors. Ulinastatin significantly ameliorated renal microcirculation perfusion at 12 hours and 24 hours in both the cortex and medulla.

Autophagy and vascular endothelial-cadherin changes in the kidney

We observed autophagosomes in the renal tubules and glomerular endothelium with a transmission electron microscope. In the sepsis group, autophagosomes were observed in renal tubular epithelial cells, and autophagosomes and lysosomes were fusing (Fig. 4A). We observed the same locations in the ulinastatin group, but no obvious autophagosomes were found (Fig. 4A). We did not observe autophagosomes in glomerular endothelial cells, both in the sepsis group and ulinastatin group, and two groups of glomerular endothelial cells were found to be partially thickened. When autophagy is formed, the cytoplasmic LC3 (i.e., LC3-I) enzymatically decomposes a small polypeptide and transforms it into an autophagosome membrane type (i.e., LC3-II). Therefore, LC3II could be used to estimate the level of autophagy. We quantified the expression of autophagy in the kidneys using Western blotting. In the sepsis and ulinastatin groups, the expression of LC3II increased (Fig. 4B). At 12 hours and 24 hours, ulinastatin was observed to inhibit the expression of LC3II in the sepsis group, and this finding was statistically different between the sepsis and ulinastatin groups ($P < 0.05$). At the same time, the

expression of VE-cadherin was reduced in the sepsis group and reached the lowest level at 24 hours. In the ulinastatin group, ulinastatin ameliorated the expression of VE-cadherin during sepsis (Fig. 4B–D). Ulinastatin may protect endothelial cell connections by inhibiting autophagy.

Histopathology

At present, there is no uniform definition of pathological changes in S-AKI. In our study, we focused on changes in the glomeruli and tubules; in the sham group, the glomerular structure was clear, and erythrocytes were observed inside some glomerular endothelial cells. The structure of the glomerulus was chaotic, and a large amount of erythrocyte stasis was observed in the glomerulus. Neutrophils were occasionally observed in the glomerulus. A small amount of lymphocyte infiltration was observed in the interstitium. In renal tubular epithelial cells, we observed cytoplasmic vacuolation, brush border injury, and protein casts in the cavity (Fig. 5A).

In the ulinastatin group, erythrocyte stasis in the glomerulus was less than that in the sepsis group. Paller scores were lower in the ulinastatin group than in the sepsis group, and there was a significant statistical difference ($P < 0.05$) (Fig. 5B). To further observe the effect of ulinastatin on the expression of vascular endothelial cells, we selected CD34 for immunohistochemistry. CD34 is expressed in normal vascular endothelial cells. In the sham group, the small blood vessels were tightly and regularly arranged, and the expression of CD34 decreased in the sepsis group, representing a decrease in the number of small blood vessels. In some areas, the vascular cavity was enlarged. Compared with the sepsis group, the number of blood vessels and the intensity of CD34 expression increased in the ulinastatin group (Fig. 5C).

Survival in each group

No rats died in the sham group; rats in the sepsis group began to die at 10 hours after surgery. If rats died within 6 hours after surgery, we considered that death was related to surgery and anesthesia. Mortality increased gradually during 12–24 hours. Survival in the ulinastatin group was higher than that in the sepsis group, but the difference was not significant ($P > 0.05$) (Fig. 6).

Figure 6: Survival analysis. After sepsis induction, all animals died within 48 hours; the mortality rate is 60%. In the ulinastatin group, the mortality rate is 55%. All animals in the sham group survived.

Discussion

In the present study, we used the typical sepsis model of CLP that closely simulates peritonitis caused by appendix perforation in the clinical setting. In this model, we observed similar hemodynamic and systemic inflammatory responses in the rats.

In the current experiment, we used non-invasive methods to measure macro- and micro-hemodynamic changes in septic rats. We observed an increase in the MAP and heart rate, but no significant changes in lactic acid at 0–6 hours after surgery; the TNF-α and IL-1β levels increased significantly at 3 hours, and the IL-6 level slightly increased. These findings indicate severe systemic inflammation postoperatively.

Some previous studies have shown that increased S-TM levels are indicative of endothelial injury and severe sepsis, and they are correlated with disseminated intravascular coagulation[25]; the S-TM level was also an independent predictive biomarker for the development of AKI[26]. In our study, the S-TM level significantly increased at 3 hours, indicating that endothelial cell damage began to appear in the early stage of sepsis. However, VE-cadherin expression had not yet changed. Previous studies have shown that the urine NGAL level has a high sensitivity and specificity for diagnosing S-AKI[27]. Based on a combination of the creatinine and urine NGAL levels, we can conclude that AKI appears in the early stage of sepsis.

We divided the time into two stages to observe the various parameters. 1) First period (0–6 hours). We observed an increase in the MAP, heart rate, and no significant changes in the lactic acid level. Creatinine and blood urea nitrogen levels increased at 3 hours and then decreased at 6 hours. Ultrasonography showed that at 3 hours, the RBF decreased and the RI increased in the sepsis group compared with the sham group, and returned to normal levels at 6 hours. At the same time, renal cortical and medullary blood perfusion (PE) did not show obvious changes. The cortical mTT was prolonged at 6 hours in the sepsis group, combined with changes in the MAP and RBF, and this is considered to be related to the increase in cortical blood flow at this time. 2) Second period (12–24 hours). The MAP and heart rate continued to decrease, reaching its lowest point at 24 hours. Simultaneously, lactic acid levels also increased, exhibiting a state of hypovolemia. We found that the MAP decreased at 12 hours, but the RBF did not decrease significantly, and the renal artery vascular RI and PI decreased, suggesting abnormal vascular function. The cortical PE showed no obvious decrease, but the medullary PE was reduced in the sepsis group compared with that in the sham group. Blood perfusion of the cortex and medulla was greatly reduced. The mTT and TTP were prolonged, especially at 24 hours. S-AKI is a complex physiological and pathological process, and there may be many different hemodynamic states. The trend of changes in the heart rate, creatinine level, and urea nitrogen level in our study is similar to the result obtained by Professor Nishkantha Arulkumaran in rats receiving fluid resuscitation[28]. Controversy always exists regarding changes in the cortex and medulla during S-AKI. A pilot study of AKI after cardiac surgery showed that cortical perfusion decreased by approximately 50%, and it did not report related data of medullary perfusion[29]. In a conscious large animal model of sheep with hyperdynamic septic shock with AKI, cortical perfusion was not significantly changed, but medullary perfusion decreased[30]. In our study, both cortical and medullary perfusion decreased, but the changes were not synchronized.

VE-cadherin is an important determinant of microvascular integrity *in vivo*[31]. In our experiments, we found that deterioration of renal function was accompanied by a decrease in VE-cadherin expression. CD34 is a highly glycosylated 115- to 120-kD monomeric surface protein that is a member of the cadherin family[32], and is selectively expressed on hematopoietic progenitor cells and the small vessel endothelium of various tissues. Both VE-cadherin and CD34 have vascular specificity and are an important part of the adhesion junction. In the present study, the expression of both proteins was reduced. VE-cadherin is transferred between the cell membrane and cytoplasm through internalization[33], autophagy activates phagocytic ability, and the circulating VE-cadherin vesicles in the cell may be phagocytosed, resulting in a decrease in the expression of VE-cadherin.

Previous studies have proven that ulinastatin can protect endothelial cells and organ functions, as follows: 1) ulinastatin can inhibit various serine proteases and factors IXa, Xa, Xia, and XIIa[34]; 2) ulinastatin blunts the increase of proinflammatory cytokines and inhibits the secretion of pro-inflammatory cytokines IL-6 and IL-8[35]; and 3) ulinastatin also downregulates stimulated arachidonic acid metabolism, such as thromboxane B2 production *in vitro* by modulating TNF-α production via the inhibition of early growth response factor[36].However, the mechanism by which ulinastatin protects microcirculation is not yet fully understood. In our study, we found that after the application of ulinastatin, the expression of VE-cadherin increased compared with that in the sepsis group. Immunohistochemistry of CD34 suggested that the number of small blood vessels after the application of ulinastatin was increased compared with that in the sepsis group. The present study showed that the expressions of adhesion junction proteins such as VE-cadherin and CD34 were decreased in the kidney tissues of rats with CLP-induced sepsis when compared with the sham group. Evidently, ulinastatin treatment reversed these changes; in other words, the expression of the above-mentioned adhesion junctional proteins was restored to varying extents. This phenomenon has been confirmed in cell experiments: ulinastatin can stabilize the barrier function of vascular endothelia[37]. Previous studies have shown that ulinastatin inhibits autophagy, and in myocardial IR injury, ulinastatin exhibits a myocardial protective effect against IR injury, but ulinastatin was found to downregulate the LC3-II protein expression[38]. Ulinastatin exerts protective effects against lipopolysaccharide-induced cardiac dysfunction, and may be associated with its anti-inflammatory and anti-autophagic activity[39].

In the present study, although the application of ulinastatin can improve the blood perfusion of the renal microcirculation at several time points, there was no significant statistical difference in the survival rate between the sepsis and ulinastatin groups. We consider this to be related to the non-application of antibiotics and failure to perform fluid resuscitation in time. Perhaps changing the dosage and frequency of administration can have an impact on the survival rate.

This study used CEUS to observe blood perfusion of the renal cortex and medulla during sepsis in rats in real time, and we found that changes in renal artery blood flow are not exactly the same as changes in microcirculation. It may be possible to use this technology to assess renal microvascular blood perfusion in the early stage of sepsis, which can further reduce the occurrence of AKI. The limitations of this experiment are as follows: 1) it was only an observational experiment, and the mechanism of the effect of ulinastatin on improving microcirculation has not been studied. 2) This experiment lacked invasive means to monitor the dynamics of academic qualifications, and we could not verify the ultrasound results. 3) Because of the small number of experimental animals, it was not possible to perform fluid resuscitation in time based on hemodynamics, and we could not fully simulate the clinical situation.

At present, monitoring of microcirculation blood perfusion and oxygenation in real time still needs to be explored further. Ulinastatin, a potential drug for the treatment of sepsis, plays an important role in inhibiting autophagy expression and verifying factors, and research on the mechanisms of inflammation, autophagy, and microvascular permeability may help to better protect kidney function in S-AKI.

Conclusions

This study provides specific experimental and ultrasound imaging evidence that ulinastatin is an effective drug that can protect the adherens junctions of endothelial cells and reduce the microcirculation dysfunction caused by sepsis. The mechanisms responsible for these effects, at least in part, involve the inhibition of autophagy via suppression of inflammatory factors during sepsis.

Declarations

Ethical Approval and Consent to participate

All rat experiments were approved by the Bioethics Committee of Beijing Friendship Hospital, Capital Medical University.

Consent for publication

Not applicable.

Availability of supporting data

The data used to support the findings of this study are available from the corresponding author upon request

Competing interests

The authors declare that there is no conflict of interest regarding the publication of this article.

Funding

This work was supported by the National Natural Science Foundation of China [81471849].

Authors' contributions

Ang Li, Meili Duan and Xiaojun Ji contributed to the study design and the interpretation of the results. Tian Li completed the experiment, conducted the data analysis, and contributed to the interpretation of results. All authors contributed to the manuscript and read and approved the final manuscript.

Acknowledgements

We gratefully acknowledge the help of our supervisor, Professor Mei Li Duan, who offered valuable suggestions for this study. We also thank Xu Qing (Department of Ultrasound, Capital Medical University) for experimental assistance and for providing the contrast-enhanced ultrasonography analysis software.

References

1. Peerapornratana S, Manrique-Caballero CL, Gómez H, Kellum JA: **Acute kidney injury from sepsis: current concepts, epidemiology, pathophysiology, prevention and treatment**. *Kidney International* 2019, **96**(5).
2. Bagshaw SM, Uchino S, Bellomo R, Morimatsu H, Morgera S, Schetz M, Tan I, Bouman C, Macedo E, Gibney N: **Septic acute kidney injury in critically ill patients: clinical characteristics and outcomes**. *Hong Kong Journal of Nephrology* 2015, **17**(2):S99-S99.
3. Bouchard J, Acharya A, Cerda J, Maccariello ER, Madarasu RC, Tolwani AJ, Liang X, Fu P, Liu ZH, Mehta RL: **A Prospective International Multicenter Study of AKI in the Intensive Care Unit**. *Clinical Journal of the American Society of Nephrology Cjasn* 2015:1324.
4. Hoste EAJ, Bagshaw SM, Bellomo R, Cely CM, Colman R, Cruz DN, Edipidis K, Forni LG, Gomersall CD, Govil D *et al*: **Epidemiology of acute kidney injury in critically ill patients: the multinational AKI-EPI study**. *Intensive Care Medicine* 2015, **41**(8):1411-1423.
5. Uchino S, Kellum JA, Bellomo R, Doig GS, Ronco C: **Acute Renal Failure in Critically Ill Patients: A Multinational, Multicenter Study**. *JAMA The Journal of the American Medical Association* 2005, **294**(7):813-818.
6. Bellomo R, Kellum JA, Ronco C, Wald R, Schneider A: **Acute kidney injury in sepsis**. *Intensive Care Medicine* 2017, **43**(3):1-13.
7. Haddy FJ: **Acute renal failure and sepsis**. *New England Journal of Medicine* 2004, **351**(22):2347-2349; author reply 2347-2349.
8. Wu L, Gokden N, Mayeux PR: **Evidence for the Role of Reactive Nitrogen Species in Polymicrobial Sepsis-Induced Renal Peritubular Capillary Dysfunction and Tubular Injury**. *Journal of the American Society of Nephrology* 2007, **18**(6):1807-1815.
9. Bulent, Ergin, Aysegul, Kapucu, Cihan, Demirci-Tansel, Can, Ince: **The renal microcirculation in sepsis**. *Nephrology, dialysis, transplantation : official publication of the European Dialysis and Transplant Association - European Renal Association* 2015.
10. Zafrani L, Payen D, Azoulay E, Ince C: **The Microcirculation of the Septic Kidney**. *Seminars in Nephrology* 2015, **35**(1):75-84.
11. Dejana E, Orsenigo F, Molendini C, Baluk P, Mcdonald DM: **Organization and signaling of endothelial cell-to-cell junctions in various regions of the blood and lymphatic vascular trees**. *Cell & Tissue Research* 2009, **335**(1):17-25.
12. Giannotta M, Trani M, Dejana E: **VE-cadherin and endothelial adherens junctions: active guardians of vascular integrity**. *Developmental Cell* 2013, **26**(5):441-454.
13. Vestweber D: **VE-Cadherin The Major Endothelial Adhesion Molecule Controlling Cellular Junctions and Blood Vessel Formation**. *Arterioscler Thromb Vasc Biol* 2008, **28**(2):223-232.
14. Schaaf MB, Houbaert D, Meçe O, Agostinis P: **Autophagy in endothelial cells and tumor angiogenesis**. *Cell Death and Differentiation* 2019.
15. Jiang M, Wei Q, Dong G, Komatsu M, Su Y, Dong Z: **Autophagy in proximal tubules protects against acute kidney injury**. *Kidney International* 2012, **82**(12):1271-1283.

16. Matsuda J, Namba T, Takabatake Y, Kimura T, Takahashi A, Yamamoto T, Minami S, Sakai S, Fujimura R, Kaimori J-y *et al*: **Antioxidant role of autophagy in maintaining the integrity of glomerular capillaries**. *Autophagy* 2018, **14**(1):53-65.
17. Atal SS, Atal S: **Ulinastatin – a newer potential therapeutic option for multiple organ dysfunction syndrome**. *Journal of Basic & Clinical Physiology & Pharmacology* 2016, **27**(2):91-99.
18. Liu S, Xu J, Gao Y, Shen P, Xia S, Li Z, Zhang M: **Multi-organ protection of ulinastatin in traumatic cardiac arrest model**. *World journal of emergency surgery : WJES* 2018, **13**:51.
19. Wang Y, Peng C, Zhang Z, Shi J, Li H: **Intravenous infusion of ulinastatin attenuates acute kidney injury after cold ischemia/reperfusion**. *International Urology and Nephrology* 2019, **51**(25).
20. Munoz CJ, Lucas A, Williams AT, Cabrales P: **A Review on Microvascular Hemodynamics: The Control of Blood Flow Distribution and Tissue Oxygenation**. *Critical care clinics* 2020, **36**(2):293-305.
21. Rossi C, Artunc F, Martirosian P, Schlemmer HP, Schick F, Boss A: **Histogram analysis of renal arterial spin labeling perfusion data reveals differences between volunteers and patients with mild chronic kidney disease**. *Investigative Radiology* 2012, **47**(8):490.
22. Harrois A, Duranteau J: **Contrast-enhanced ultrasound: a new vision of microcirculation in the intensive care unit**. *Critical Care* 2013, **17**(4).
23. Xu HX, Lu MD: **The current status of contrast-enhanced ultrasound in China**. *Journal of Medical Ultrasonics* 2010, **37**(3):97-106.
24. Paller MS, Hoidal JR, Ferris TF: **Oxygen free radicals in ischemic acute renal failure in the rat**. *The Journal of Clinical Investigation* 1984, **74**(4):1156-1164.
25. Lin SM, Wang YM, Lin HC, Lee KY, Huang CD, Liu CY, Wang CH, Kuo HP: **Serum thrombomodulin level relates to the clinical course of disseminated intravascular coagulation, multiorgan dysfunction syndrome, and mortality in patients with sepsis**. *Crit Care Med* 2008, **36**(3):683-689.
26. Katayama S, Nunomiya S, Koyama K, Wada M, Koinuma T, Goto Y, Tonai K, Shima J: **Markers of acute kidney injury in patients with sepsis: the role of soluble thrombomodulin**. *Critical Care* 2017, **21**(1):229.
27. Böttiger B, Bernhard M, Knapp J, Nagele P: **Influence of EMS-physician presence on survival after out-of-hospital cardiopulmonary resuscitation: systematic review and meta-analysis**. *Critical Care* 2015.
28. Arulkumaran N, Sixma ML, Jentho E, Ceravola E, Singer M: **Sequential Analysis of a Panel of Biomarkers and Pathologic Findings in a Resuscitated Rat Model of Sepsis and Recovery**. *Critical Care Medicine* 2017, **45**(8):e821-e830.
29. Schneider AG, Goodwin M, Schelleman A, Bailey M, Bellomo R: **Contrast-enhanced ultrasound to evaluate changes in renal cortical perfusion around cardiac surgery: a pilot study**. *Critical Care* 2013, **17**(4):R138.
30. Calzavacca P, Evans RG, Bailey M, Bellomo R, May CN: **Cortical and Medullary Tissue Perfusion and Oxygenation in Experimental Septic Acute Kidney Injury**. *Critical Care Medicine* 2015, **43**(10):431-439.

31. Corada M, Mariotti M, Thurston G, Smith K, Kunkel R, Brockhaus M, Lampugnani MG, Martin-Padura I, Stoppacciaro A, Ruco L *et al*: **Vascular endothelial–cadherin is an important determinant of microvascular integrity in vivo**. *Proceedings of the National Academy of Sciences* 1999, **96**(17):9815-9820.
32. Gangenahalli GU, Singh VK, Verma YK, Gupta P, Sharma RK, Chandra R, Luthra PM: **Hematopoietic stem cell antigen CD34: role in adhesion or homing**. *Stem Cells & Development* 2006, **15**(3):305-313.
33. Basagiannis D, Zografou S, Murphy C, Fotsis T, Christoforidis S: **VEGF induces signalling and angiogenesis by directing VEGFR2 internalisation through macropinocytosis**. *Development* 2016, **143**(22):e1.1-e1.1.
34. Pugia MJ, Valdes R, Jortani SA: **Bikunin (Urinary Trypsin Inhibitor): Structure, Biological Relevance, And Measurement**: Advances in Clinical Chemistry; 2007.
35. Han JI: **Urinary trypsin inhibitor: miraculous medicine in many surgical situations?** *Korean Journal of Anesthesiology* 2010, **58**(4):325-327.
36. Xu CE, Zhang MY, Zou CW, Guo L: **Evaluation of the Pharmacological Function of Ulinastatin in Experimental Animals**. *Molecules* 2012, **17**(8).
37. Wei F, Liu SY, Luo L, Gu NN, Zeng Y, Chen XY, Xu S, Zhang D: **Anti-inflammatory mechanism of ulinastatin: Inhibiting the hyperpermeability of vascular endothelial cells induced by TNF-α via the RhoA/ROCK signal pathway**. *International Immunopharmacology* 2017, **46**(Complete):220-227.
38. Xiao J, Zhu X, Ji G, Yang Q, Kang B, Zhao J, Yao F, Wu L, Ni X, Wang Z: **Ulinastatin protects cardiomyocytes against ischemia-reperfusion injury by regulating autophagy through mTOR activation**. *Molecular Medicine Reports* 2014, **10**(4):1949-1953.
39. Zhao, Zhang, Gao, Ding, Yang, Kuai: **Ulinastatin attenuates lipopolysaccharideinduced cardiac dysfunction by inhibiting inflammation and regulating autophagy**. *Experimental and Therapeutic Medicine* 2020.

Figures

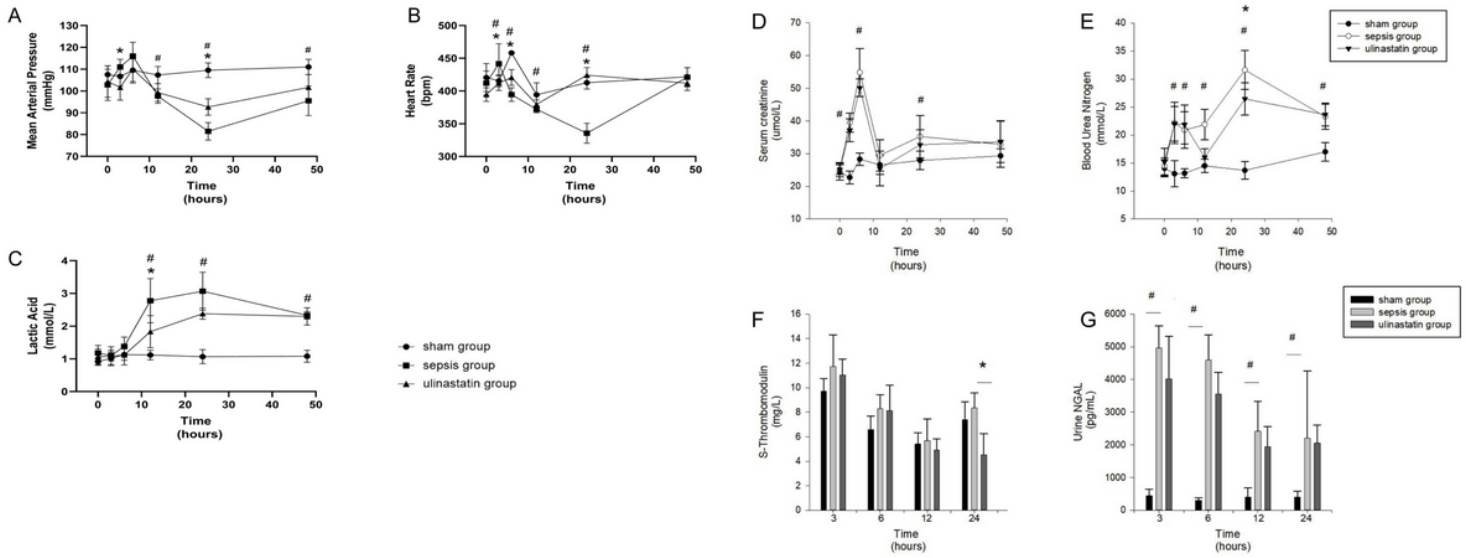

Figure 1

Systemic hemodynamics and renal function in septic rats. (A–B) The mean arterial pressure and heart rate values measured at different time points. (C) The lactate levels based on blood sampling from the tail vein. (D–F) The creatinine, blood urea nitrogen, and S-thrombomodulin serum levels are shown. (G) The neutrophil gelatinase-associated lipocalin (NGAL) levels based on urine sampling collected through a metabolic cage. # sepsis group versus (vs.) sham group, $P < 0.05$, * ulinastatin group vs. sepsis group, $P < 0.05$ ($n = 6$).

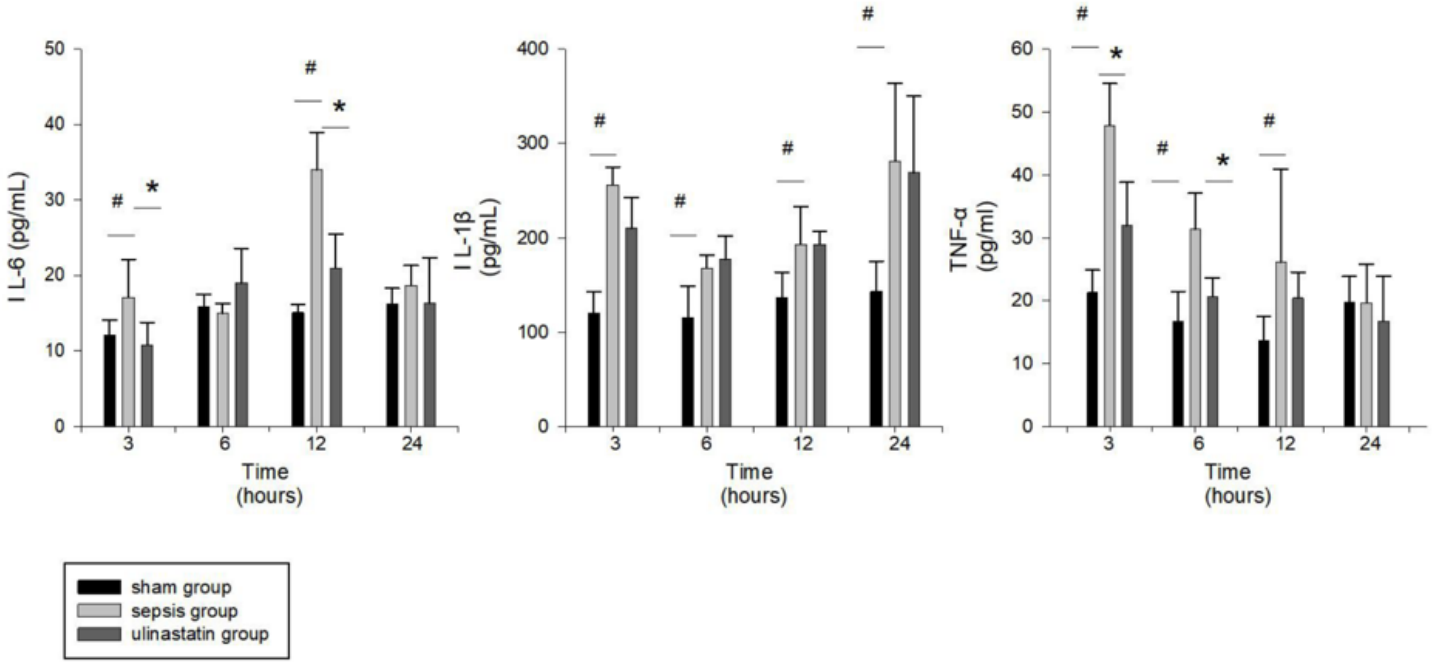

Figure 2

Inflammatory factors in septic rats at different time points. Blood sampling was collected from the renal artery, and enzyme-linked immunosorbent assay was used to quantify the inflammatory factors. # sepsis group versus [vs.] sham group, P < 0.05, * ulinastatin group vs. sepsis group, P < 0.05 (n = 6).

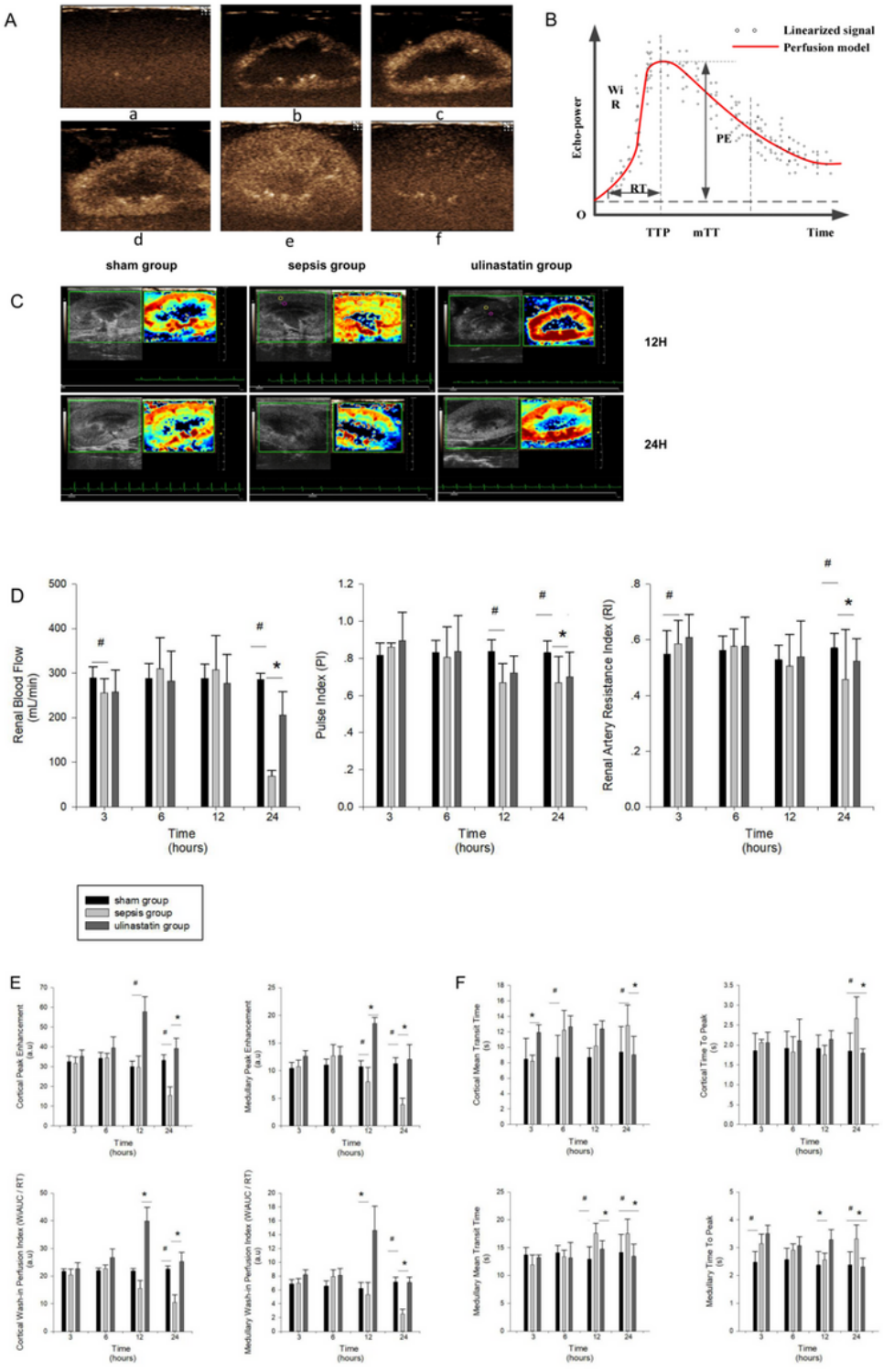

Figure 3

Contrast-enhanced ultrasound images and related parameters. (A) Renal gray-scale contrast-enhanced ultrasonography showing the real-time contrast-matched imaging technique. (a) Before injecting the

contrast agent; (b) the cortical filling period; (c) cortical enhancement period; (c) the medullary filling period; (e) the enhanced period; and (f) the dissipation period. TTP, time to peak; mTT, mean transit time; WIR, wash-in perfusion index; RT, rise time; PE, peak enhancement (B) Bolus perfusion model: Perfusion quantification represents the core of the Vevo CQ functionality and performs quantification in two steps. 1) Video data is first converted into echo-power data, a quantity directly proportional to the instantaneous concentration of the contrast agent concentration at each location in the field of view; this conversion process is called linearization. 2) The echo-power data as a function of time, or linearized signals, are then processed to assess blood perfusion, using a curve fitting approach with a parametric perfusion model. (C) The intensity before the contrast agent reached the renal parenchyma is set to zero, and the cumulative intensity is calculated. The intensity of the contrast agent is encoded by a particular color on the parameter color scale. The medulla of the renal cortex is shown in cyan and blue, and the cortex is shown in red and yellow. In the sham group, the boundary between the renal cortex and medulla is obvious. Abnormal perfusion is observed in the sepsis group, and several renal cortical locales are lost. In the ulinastatin group, cortical perfusion is significantly enhanced. (D) Parameters related to the left renal artery. (E–F) Renal cortical and medullary perfusion-related parameters. # sepsis group versus (vs.) sham group, $P < 0.05$, * ulinastatin group vs. sepsis group, $P < 0.05$ ($n = 6$).

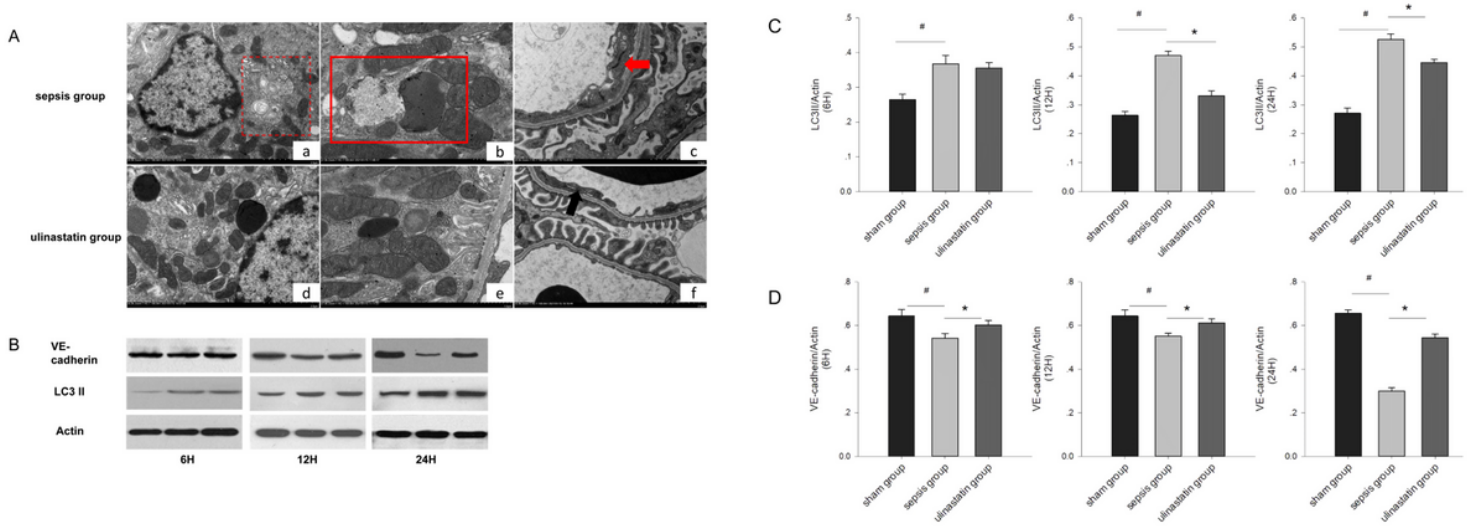

Figure 4

Transmission electron micrograph of the glomerulus, tubules, and target protein expression in the kidney. (A) (a–b) In the sepsis group, two separate autophagosomes (red dashed box) and a fusion autophagolysosome (red solid line box) are seen in the tubules. (d–e) In the ulinastatin group, no obviously autophagosomes are observed. (c, f) Partial swelling of glomerular endothelial cells is observed (thick red arrow and black arrow). (B–D) Quantification of the target protein in the kidney (vascular endothelial [VE]-cadherin and LC3II). # sepsis group versus (vs.) sham group, $P < 0.05$, * ulinastatin group vs. sepsis group, $P < 0.05$ ($n = 6$).

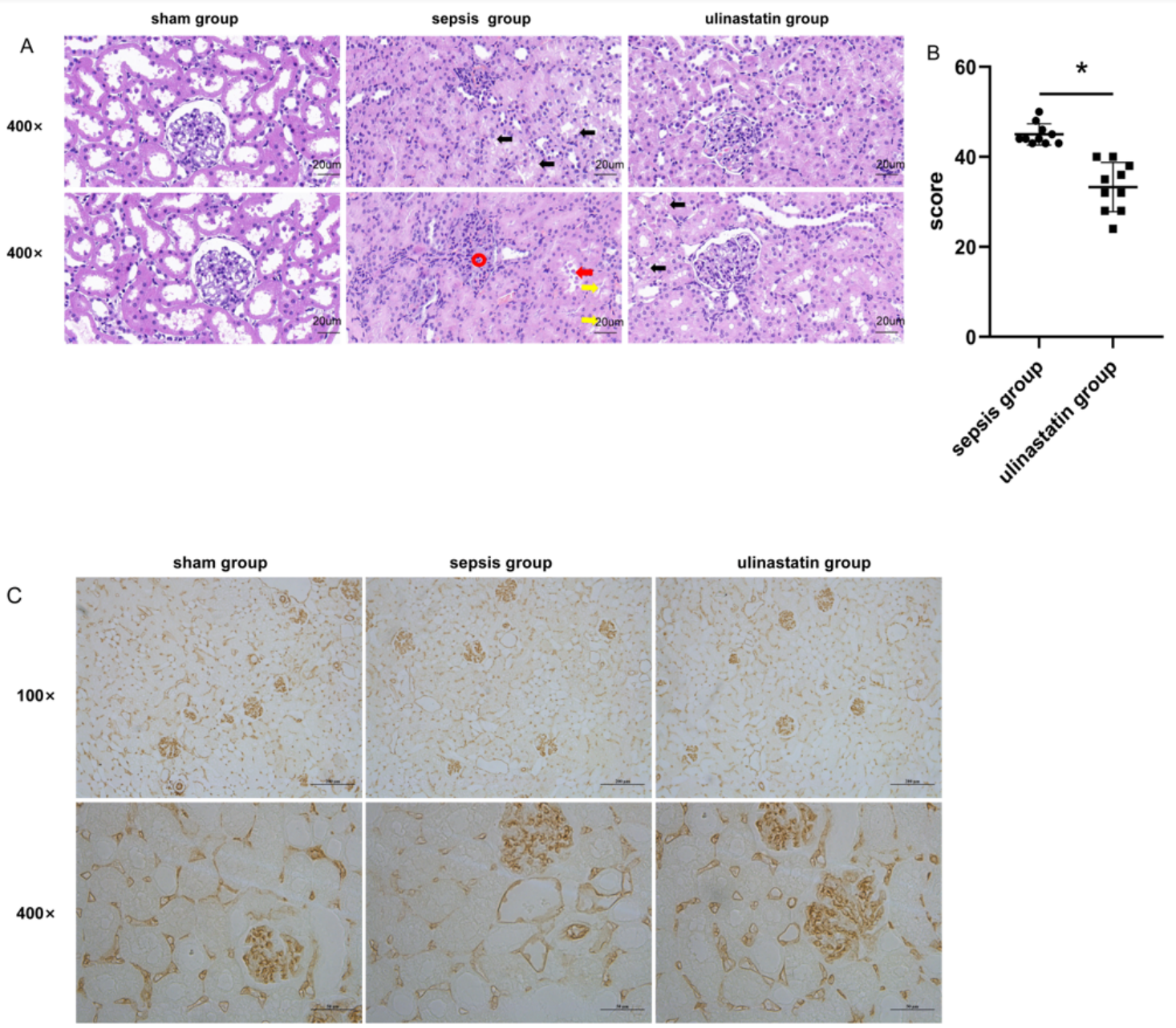

Figure 5

Histopathology of cecal ligation and puncture-induced acute kidney injury at 24 hours. (A) In the sham group, the structure of the glomeruli and tubules is obvious and clear. Erythrocyte stasis in the renal cortex, neutrophils in the renal glomerulus (red circle), protein casts in the renal tubules (red arrow), cytoplasmic vacuolization of renal tubular epithelial cells (black arrow), and brush border injury (yellow arrow) can be seen. The change of pathology in the ulinastatin group was mild compared with the sepsis group. Hematoxylin-eosin stain, bar 20 μm. (B) The Paller score was lower in the ulinastatin group than in the sepsis group ($P < 0.05$). (C) CD34 immunohistochemistry. Bar 50 μm.

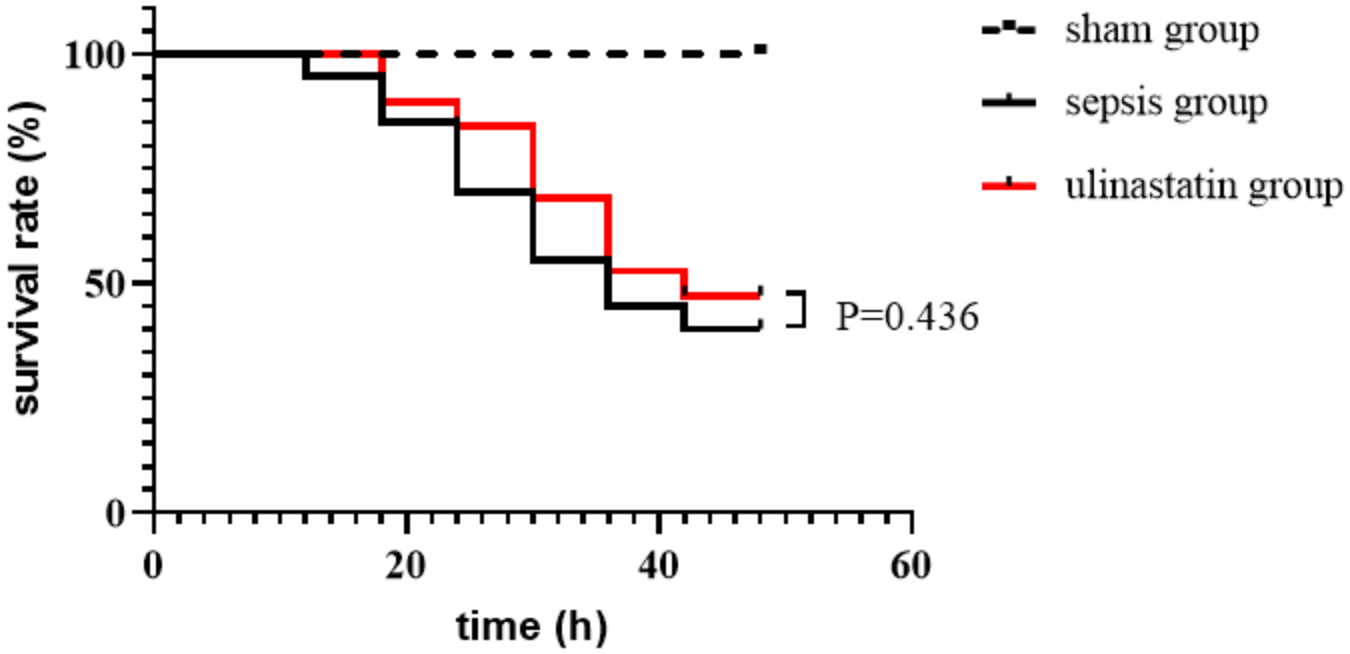

Figure 6

Survival analysis. After sepsis induction, all animals died within 48 hours; the mortality rate is 60%. In the ulinastatin group, the mortality rate is 55%. All animals in the sham group survived.